CROATICA CHEMICA ACTA CCACAA **72** (2–3) 621–643 (1999)

ISSN-0011-1643
CCA-2602 *Original Scientific Paper*

Precipitation and Dissolution Phenomena in Al-Zn Alloys*

Stanko Popović [a,**] *and Biserka Gržeta* [b]

[a] *Department of Physics, Faculty of Science, University of Zagreb, P.O. Box 162, 10001 Zagreb, Croatia*

[b] *Ruđer Bošković Institute, P.O. Box 1016, 10001 Zagreb, Croatia*

Received October 12, 1998; revised April 19, 1999; accepted April 20, 1999

The microstructure of Al-Zn alloys, with the Zn atom fraction, $x_{Zn} \leq 62\%$, has been studied in detail by XRD in dependence on the composition, temperature and previous thermal treatment. Precipitation phenomena in alloys, transferred to the supersaturated state by rapid quenching from the solid solution temperature, T_{ss}, in water at RT, have been followed in dependence on the ageing time at RT or elevated temperature. The equilibrium state, reached by ageing, has been compared with that obtained by slow cooling from T_{ss} to RT. Phase transitions, dissolution and precipitation processes in the alloys, transferred to the equilibrium state, have been studied *in situ* in dependence on temperature from RT to T_{ss}. A temperature hysteresis in reversal phase transitions has been observed on cooling from T_{ss} to RT. Repeated heating and cooling cycles have revealed different microstructure in alloys having undergone different thermal treatments between RT and T_{ss}. A change in the phase diagram of the Al-Zn system is necessary in the composition region $x_{Zn} > 50\%$.

Key words: Al-Zn alloys, solid solutions, precipitation phenomena in solids, phase transitions, phase diagram, X-ray powder diffraction.

---

* Dedicated to Professor Boris Kamenar on the occasion of his 70th birthday.

** Author to whom correspondence should be addressed.

INTRODUCTION

The microstructure, physical and chemical properties of the Al-Zn system, with respect to the composition and applied heat treatment, have been studied by many authors. Most of the collected knowledge can be found in a recent comprehensive monograph[1] edited by H. Löffler, containing about 700 references. Zinc atoms do not tend to form intermetallic phases with Al atoms, which means that the Al-Zn interactions are rather weak. The atomic radius of Al atoms amounts to 1.43 Å (1 Å = 0.1 nm), while the one of Zn is about 1.34 Å. This difference has a great influence on the microstructure of Al-Zn alloys.

Al-Zn alloys in the equilibrium state, formed after a prolonged ageing, say at room temperature (RT, 298 K), are two-phase systems, consisting of the fcc α-phase (the matrix, M) having $x_{Al} \approx 99\%$, and the hexagonal β(Zn)-phase (the precipitates) having $x_{Zn} \approx 99.5\%$. This means that the solid solubility of Zn in Al is 0.85%, while the one of Al in Zn is less than 0.5% at RT.[1] The solubility of Zn in Al increases with temperature and reaches ≈ 67% at ≈ 655 K, being the highest among all elements.[1] Al-Zn alloys rapidly quenched from the solid-solution temperature, T_{ss} [*e.g.* T_{ss} = 625 K for the alloy with the initial x_{Zn} of 39.5%], to RT are metastable and decompose to a two-phase system (at least up to $x_{Zn} \approx 44\%$), consisting of the fcc α(M/GPZ)- phase in a metastable equilibrium with a dense system of Guinier-Preston zones (GPZ), having $x_{Zn} \approx 70\%$. On ageing, at room or at elevated temperature, the decomposition of the rapidly quenched alloys (supersaturated solid solutions of Zn in Al) proceeds in a number of phase transitions. The longest decomposition sequence is the following: spherical GPZ (fcc, fully coherent with the matrix, having the radius of 1 to 2 nm) → ellipsoidal GPZ (fcc, fully coherent with M) → rhombohedrally distorted α'_R-phase (partially coherent with M, having the mean radius of the order of 10 nm) → metastable α′-phase (fcc, partially coherent with M) → β(Zn)-phase (incoherent with M).[1] The gain of free energy associated with the formation of the β(Zn) equilibrium phase is reduced with the increase of the ageing temperature. As a consequence, the number of the intermediate metastable phases during the decomposition is reduced with the decrease of the ageing temperature. For ageing at RT, one may expect even a direct transition of big GPZ to β(Zn) precipitates.[1]

The decomposition process, *i.e.* the precipitation of particular phases, GPZ, α'_R, α′ and β(Zn), is mainly governed by the quenched-in vacancies. The binding energy of the vacancy-solute atom pair is estimated as 0.13(3) eV at RT.[1] After completion of the precipitation process, the fcc α(M/β)-phase, depleted in Zn, is in a stable equilibrium with β(Zn) precipitates, which may be of a micrometer size. The ageing time necessary to reach the equilibrium

state decreases with the increase of the Zn content and the ageing temperature, the latter strongly influencing the diffusion rate of the Zn atoms inside the Al host crystal lattice.[1]

On the basis of a number of papers, most of them being referred to in Ref. 1, the phase diagram of the Al-Zn system has been established and accepted in the literature.[1,2]

Keeping in mind the mentioned experimental and theoretical evidence, the Al-Zn alloys are very suitable for studying the mechanism and kinetics of phase transitions in supersaturated solid solutions.

In spite of the very extensive literature data on the Al-Zn system, a need arose recently to perform a more detailed and accurate investigation of the microstructure in dependence on the composition, temperature and thermal treatment of the alloys. Therefore, the Al-Zn alloys, having undergone different thermal treatments, were studied in detail by means of X-ray powder diffraction (XRD). The alloys of different composition, quenched rapidly from T_{ss} to RT, were subjected to ageing at RT or at elevated temperature, and the precipitation processes, that is, the decomposition of the supersaturated solid solutions, were followed. Also, alloys of different composition, having reached the equilibrium state, were subjected to a gradual change of temperature, from RT to T_{ss} and back to RT, and their microstructure was followed *in situ* by XRD. These recent investigations have proved that accurate measurements of the positions of diffraction lines and a study of diffraction line profiles are very useful to obtain new information, *e.g.* about the zinc content in the matrix, M, for different types of precipitates, P, in contact with it, and the effect of strains occurring at the M/P interface on the lattice constant of M, $a[\alpha(M/P)]$, on the lattice constant of the intermediate phase α', $a(\alpha')$, and the lattice constant of the solid solution, $a(\alpha_{ss})$. Also, the present study has checked the validity of the phase diagram of the Al-Zn system.

EXPERIMENTAL

A series of Al-Zn alloys, with x_{Zn} = 4.5, 8, 15, 20, 24, 26, 35, 38, 40, 44, 48, 54 and 62%, were produced from components of purity 4N. The samples for XRD were as follows: (i) thin foils of about 0.15 mm in thickness, prepared by stepwise rolling with immediate annealing (foils, for short), (ii) fine powders prepared by filing the foils and having particle sizes between 10 and 50 μm (powders, for short), (iii) thin needles, cut-off from the foils, with approximate size of $5 \times 0.10 \times 0.15$ mm^3 (needles, for short). The foils exhibited a strong preferred orientation of crystal grains, as evidenced from relative diffraction line intensities which changed statistically (especially at high Bragg angles) from one foil to another. On the other hand, powdered samples showed a random orientation of crystal grains.

The XRD patterns of the foils and powders were taken using a Philips counter diffractometer having a high-temperature attachment, a proportional counter and a graphite monochromator, with Cu-Kα radiation. The needles were investigated by means of a Debye-Scherrer camera, thus utilizing the spectral doublets of matrix diffraction lines 511+333 and 422 at the Bragg angles > 81° and > 68°, respectively. All precautions were taken into account in order to minimize the systematic aberrations influencing the diffraction line positions,[3] as well as in manipulation with the needles, preventing any transfer of heat to them. The samples were exposed either to the standard air pressure of 10^5 Pa, or to a low air pressure of 10^{-3} Pa, but no effect of oxidation was observed by XRD. Several experiments were run with each alloy and quite reproducible results were obtained.

Various heat treatments were applied:

– The samples were annealed in the region of the solid solution temperatures, from 570 K to 770 K, for 1 h and quenched inside the furnace in water at RT. A 1 m long tube full of water was inserted into the furnace just before the quench; the free-fall path of the sample to the water surface was about 10 mm. The powders were wrapped in a thin foil having the thickness of 0.05 mm, perforated with hundreds of small holes made using a needle in order to increase the quenching rate. The quenching rate was estimated as 10^5 K s^{-1}. The diffraction patterns in the Debye-Scherrer camera were taken within 3 hours after quenching, or the profiles of prominent diffraction lines were scanned by means of the counter diffractometer within 30 min.

– The samples were slowly cooled over two days within the furnace from the temperature in the region of solid solution to RT.

– The as-quenched samples were stored at 520 K for 5 days and subsequently cooled to RT over 15 days.

– The as-quenched samples were stored (aged) at RT or at elevated temperature (up to 350 K) for the time required (two days for alloys with high Zn contents, up to 1 year for alloys with small Zn contents).

– The samples, having reached the equilibrium state (after a prolonged ageing) were heated from RT to the solid solution temperature and then cooled to RT, at a rate of ≈ 2 K min^{-1}. The heating/cooling of the sample was stopped at a series of temperatures in order to scan prominent diffraction line profiles.

More experimental details were given in the previous papers.[4–10]

RESULTS AND DISCUSSION

Precipitation Processes at RT after Quenching

Characteristic parts of diffraction patterns obtained by the Debye-Scherrer camera for a series of alloys immediately after quenching are shown in Figure 1. For comparison, the patterns of pure and annealed Al and the pattern of a slowly cooled alloy with x_{Zn} = 40% are also shown in Figure 1. Prominent diffraction lines of pure Al and of the alloys with x_{Zn} = 38 and 40%, taken by the counter diffractometer within 30 min after quenching, are shown in Figure 2.

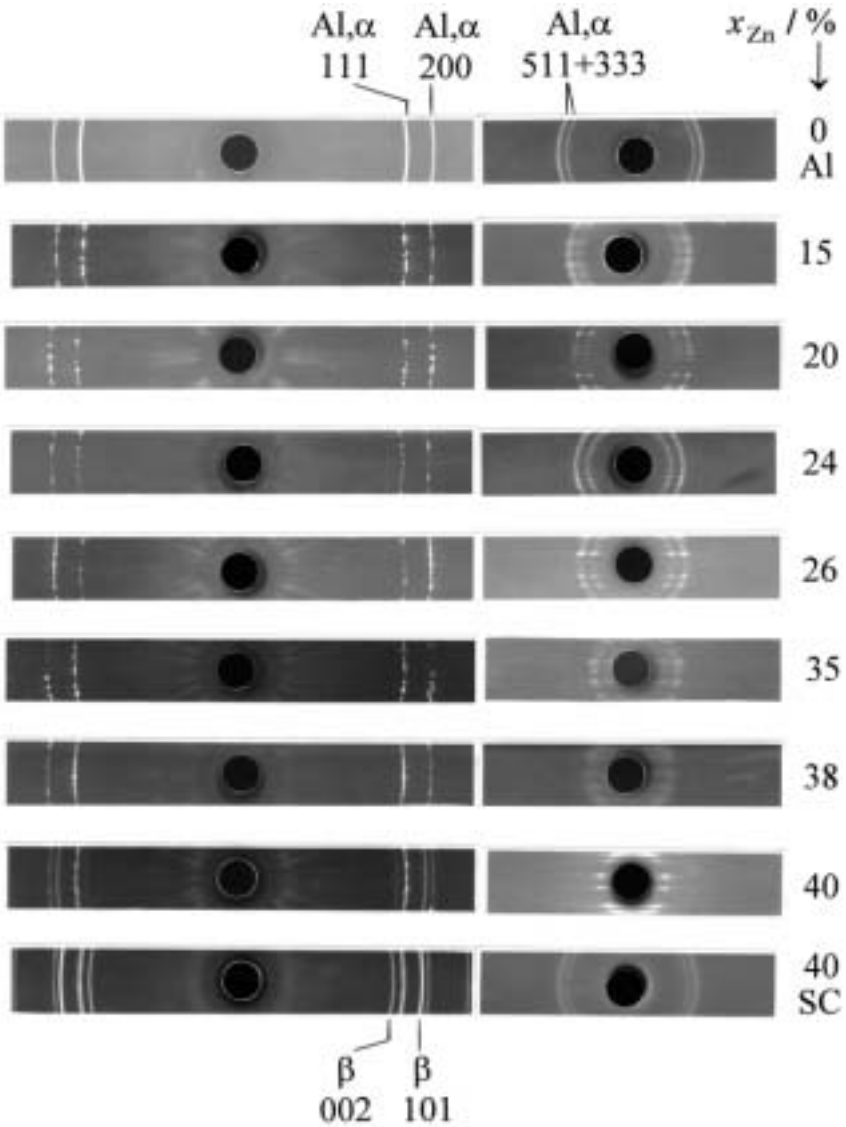

Figure 1. Debye-Scherrer diffraction patterns of annealed pure Al and a series of Al-Zn alloys taken immediately after quenching from 673 K in water at RT. The pattern of the slowly cooled (SC) Al-Zn (x_{Zn} = 40%) alloy is also shown. Samples: needles. Radiation: monochromatized Cu-Kα.

Immediately after quenching the alloys are decomposed into two phases, *i.e.* the fcc α-matrix, α(M/GPZ) and a fairly dense system of GP zones, which are in a metastable equilibrium state with each other. One can see in Figures

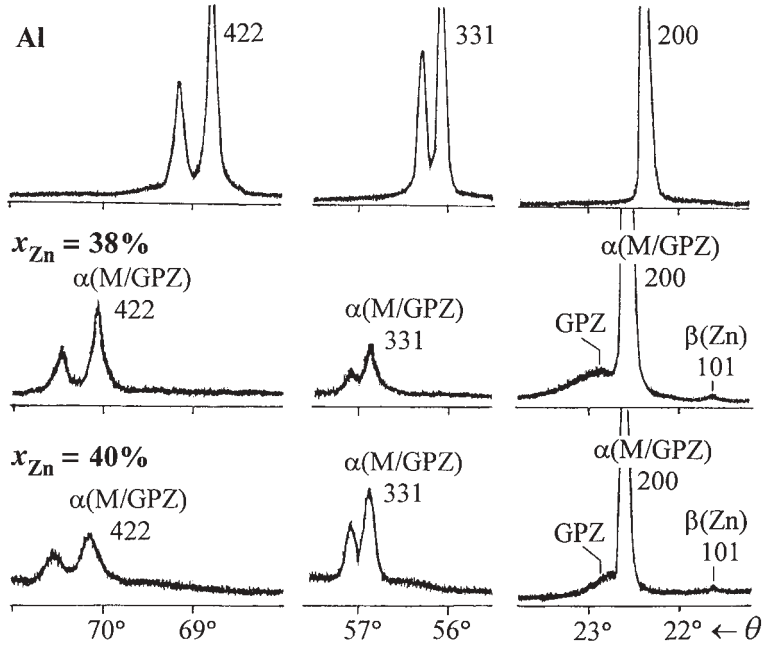

Figure 2. Prominent diffraction lines of annealed pure Al and of the alloys with x_{Zn} = 38 and 40% taken during 30 min of ageing at RT after quenching from 673 K in water at RT. The arrows indicate the diffraction effect from GP zones. Samples: fine powder.

1 and 2 that diffraction lines of α(M/GPZ) are shifted to Bragg angles which are higher than those of pure Al. This shift increases with the initial content of Zn, x_{Zn}, in the alloys. Phase β(Zn) is not present in the alloys immediately after quenching, at least up to $x_{Zn} \approx 40\%$. Even in the alloys with fairly high x_{Zn} of 38 and 40%, the strongest diffraction line of β(Zn), 101, is hardly visible in Figure 2, and its appearance is due to the β(Zn) precipitates formed while taking the diffraction pattern (30 min). Diffraction line 101 of β(Zn) is more pronounced in Figure 1 for the alloy with x_{Zn} = 40% because of the longer time (3 h) of taking the diffraction pattern. One can also see in Figure 1 that the diffraction lines of the fcc α(M/GPZ)-phase are more or less spotty due to coarse crystal grains formed during the heating to the solid-solution temperature (before quenching), while diffraction lines of fine β(Zn) precipitates are continuous (the quenched and slowly cooled alloy with x_{Zn} of 40%).

The lattice constants of α(M/GPZ) at RT are given in Table I. One can see that a[α(M/GPZ)] decreases practically linearly with increasing the initial content of Zn in the alloys. This dependence is in agreement with the

TABLE I

a[α(M/GPZ)] as a function of the initial zinc content, x_{Zn}, of several Al-Zn alloys in the as-quenched state at RT[a]

x_{Zn} / %	a[α(M/GPZ)] / Å
0 (pure Al)	4.0494(3)
4.5	4.0465(3)
8	4.0426(5)
15	4.0346(5)
20	4.0330(5)
24	4.0287(5)
26	4.0272(5)
35	4.0190(7)
38	4.0171(7)
40	4.0123(8)
44	4.0094(8)
48	no GP zones

[a] The results are practically the same for both kinds of samples, needles and powders.[5,10] For comparison, the lattice constant of pure Al is also given.

data given in Ref. 11; however, that reference contains data only for $x_{Zn} < 30\%$. The alloy with $x_{Zn} = 44\%$ shows the rather diffuse spectral doublet 511+333, while the as-quenched alloy with $x_{Zn} = 48\%$ does not contain GP zones.

It is obvious from Figures 1 and 2 that, at least up to $x_{Zn} \approx 40\%$, diffraction lines of α(M/GPZ) are fairly sharp with well-separated $K\alpha_1\alpha_2$ spectral doublet components, but are little broader than those of pure Al, indicating strains in the matrix around GP zones. One can also see in Figure 2 that, at the high-angle side of diffraction lines of α(M/GPZ), there is a broad hump due to diffraction effects in GP zones. In the foils, having a strong preferred orientation of crystal grains, with planes (200) of the α-phase parallel to the foil surface, the diffraction effect from GP zones (*i.e.* diffraction line 200 from the zones) is much stronger than in the powders. Broad diffraction lines of GP zones are shifted toward higher Bragg angles from the corresponding diffraction lines of α(M/GPZ) due to a much higher Zn content in the zones than in the matrix.[5]

A decrease of the lattice constant of α(M/GPZ), in relation to pure Al, with the increase of the initial Zn content, may be explained, on the one

hand, in terms of an increased fraction of Zn dissolved in the matrix on quenching. For the alloy with x_{Zn} = 44%, the lattice constant of α(M/GPZ) is 1.0% smaller than that of pure Al. On the other hand, in the Al-Zn alloy, containing a dense system of almost spherical GP zones coherent with the matrix, there should be a continuation of the lattice planes from GP zones into the neighbouring (strained) matrix, decreasing the contribution of the coherency strains to the total free enthalpy.[4,5]

For the alloys, rapidly quenched from the solid-solution temperature to RT and aged at RT, or at a temperature below 350 K, diffraction lines of α(M/GPZ) gradually decrease in intensity, becoming little broader but not changing their angular positions. Diffraction effects from GP zones disappear with ageing. At the same time, diffraction lines of α(M/β) appear, at angular positions close to those of the α-phase in the slowly cooled alloys, as well as diffraction lines of β(Zn) at angular positions close to those of pure Zn (Figures 3, 4).[4,5] In fact, at first GP zones grow in size with ageing; as ageing proceeds on GP zones, reaching a critical size of say ten nanometers, they directly transform to β(Zn) precipitates. This is the shortest sequence of phases existing in the Al-Zn system. Similar phenomena were also observed in Al-Ag-Zn alloys.[13–15]

Diffraction lines of α(M/β) were very broad at first, due to strains around the precipitates β(Zn); as ageing proceeded they became sharper. Their intensities increase with ageing, as do the ones of β(Zn). The diffraction lines of β(Zn) are rather sharp from the very beginning. Most of the formed β(Zn)-precipitates are nucleated at GP zones. This transition may start with the formation of stacking faults or microlamellae of hcp structure on {111} planes of GP zones, resulting in $\{001\}_\beta \,||\, \{111\}_{GPZ}$, in accordance with the orientation relationship between β(Zn) and α(M/β), namely $\{001\}_\beta \,||\, \{111\}_\alpha$, $[110]_\beta \,||\, [1\bar{1}0]_\alpha$.[1] Using the lattice constants a[α(M/β)] and c(β), it follows that $3c(\beta) \approx 2\sqrt{3}\ a[\alpha(M/\beta)]$, the misfit between the corresponding spacings being 5.5%. The consequence of this is that a part of the $\{001\}_\beta$ planes of the small (plate-like) β(Zn) precipitates should be continued in the $\{111\}_\alpha$ planes, *i.e.* the platelets maintain a certain degree of coherency to the ambient matrix, resulting in a distortion of the matrix lattice surrounding the β(Zn) platelets. As the β(Zn) precipitates grow, the coherency is more and more destroyed, β(Zn) precipitates assuming shapes of prisms, polyhedra, *etc*.[5]

Figure 4 shows three stages of ageing at RT of the alloy with x_{Zn} = 38%: 30 min after quenching, with diffraction lines of α(M/GPZ) and GP zones present; 52.5 h of ageing, where diffraction lines of α(M/GPZ), α(M/β) and β(Zn) are present; and after 35 d of ageing, with diffraction lines of α(M/β) and β(Zn). One can see that the diffraction line 311 of α(M/GPZ) is sharper than 311 of α(M/β) for the ageing time of 52.5 h. This difference is more pro-

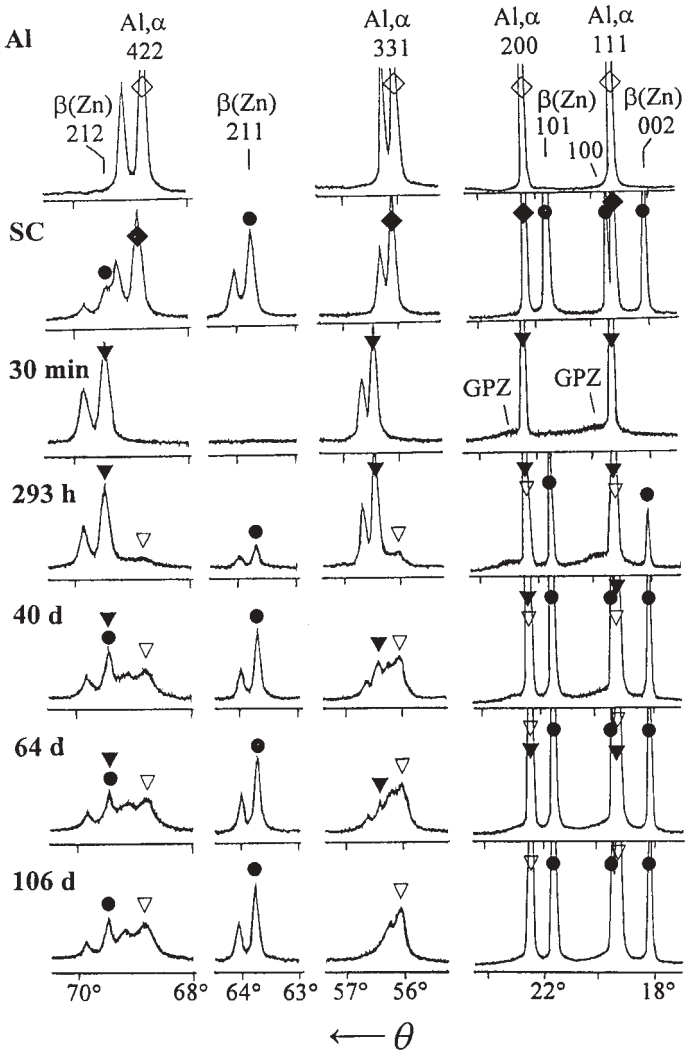

Figure 3. Essential parts of diffraction patterns of annealed pure Al, of the Al-Zn (x_{Zn} = 24%) alloy slowly cooled to RT (SC), and of the Al-Zn (x_{Zn} = 24%) alloy quenched from 653 K in water at RT and aged at RT for 30 min, 293 h, 40 d, 64, d, 106 d. Notation: ◊ = pure Al, ▼ = α(M/GPZ), ▽ = α(M/β), ♦ = α, SC, ● = β(Zn) (shown only at $K\alpha_1$ components, where the spectral components $K\alpha_1\alpha_2$ are resolved). Arrows indicate the diffraction effect from GP zones. Samples: fine powder.

nounced in Figure 5, showing the alloy with x_{Zn} = 24% after 1 d and 26 d of ageing at RT. Diffraction line 422 of α(M(GPZ) becomes a little broader with ageing due to the strained crystal lattice of the matrix around GP zones,

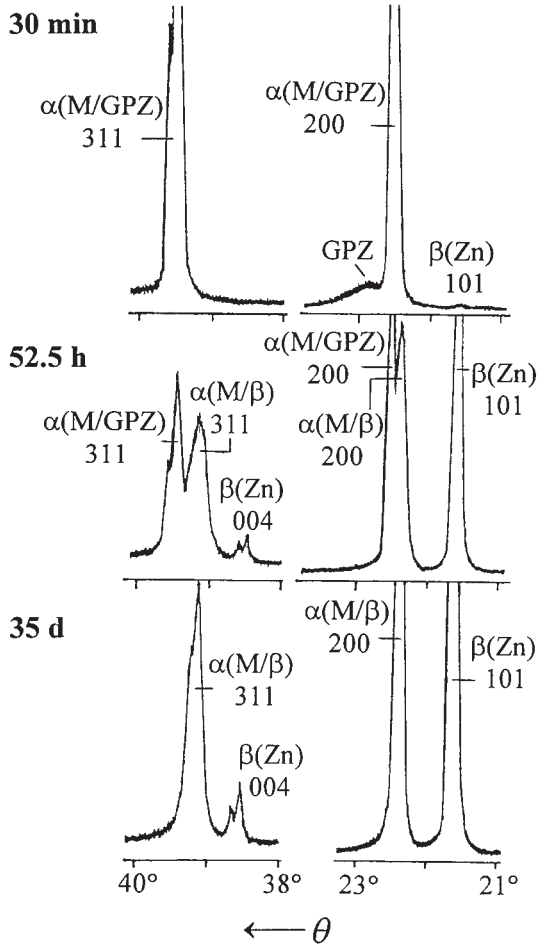

Figure 4. Diffraction lines of the Al-Zn (x_{Zn} = 38%) alloy, quenched from 673 K in water at RT and aged at RT for 30 min, 52.5 h, 35 d. Samples: fine powder.

and at a later stage of ageing due to decreased diffracting volumes. On the other hand, the diffraction line 422 of α(M/β) is very broad and not resolved into the spectral doublet components. At the same time, diffraction lines of β(Zn) are rather sharp (Figures 3 to 5), since the crystal lattice inside the β(Zn) precipitates is in an almost unstrained condition. The broadening of diffraction lines of α(M/β) is caused at early stages of ageing by small diffracting volumes, and afterwards by the strained crystal lattice of the matrix around β(Zn) precipitates, as they increase in size, due to the misfit in spacings of the phases α(M/β) and β(Zn). The sharpening of the diffraction

line 331 of α(M/β) with prolonged ageing at RT for the Al-Zn (x_{Zn} = 24%) alloy is shown in Figure 6. For the ageing time of 49 d the diffraction line 331 of α(M/β) is much broader than the one of α(M/GPZ), since the matrix around β(Zn) precipitates is much more strained than around GP zones. For the ageing time of 63 d α(M/GPZ) cannot be detected any more, but the line 331 of α(M/β) is still very broad. For the ageing time of 192 d, the diffraction line 331 of α(M/β) shows a separation into the spectral doublet components, and this takes place much later than the time at which the intensities of β(Zn) diffraction lines reach saturation (this will be shown in Figure 8). Ageing of the same alloy for 1 d at RT and subsequent ageing at 333 K accelerates decomposition. Figure 7 shows the difference in broadening between diffraction lines of β(Zn) and α(M/β) for the ageing time of 1 d and 33 d at 333 K.

The dependence of the diffraction line intensities of β(Zn) on the ageing time at RT is shown in Figure 8 for the alloy with x_{Zn} = 24%, quenched from 623 K and from 653 K in water at RT. After a prolonged ageing time, dif-

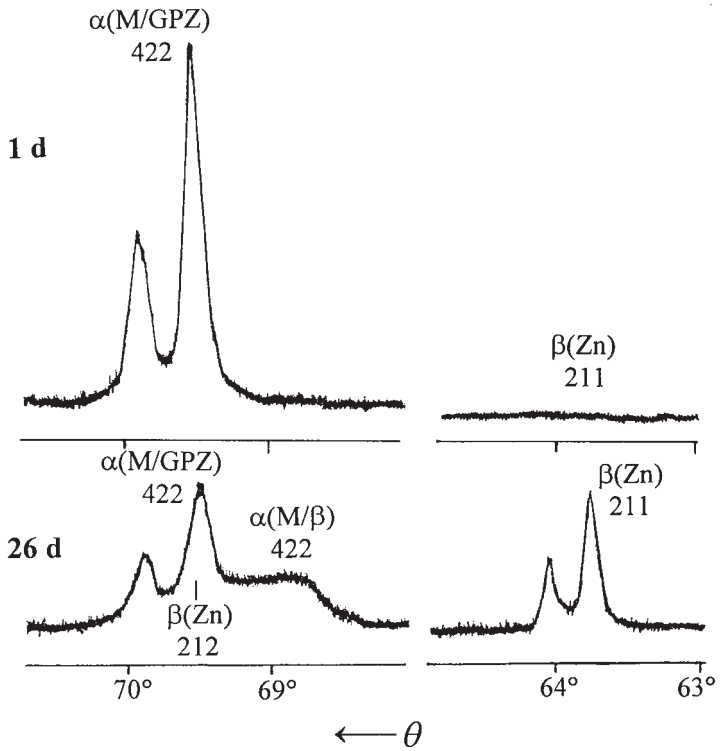

Figure 5. Diffraction lines of the Al-Zn (x_{Zn} = 24%) alloy, quenched from 673 K in water at RT and aged at RT for 1 d and 26 d. Samples: fine powder.

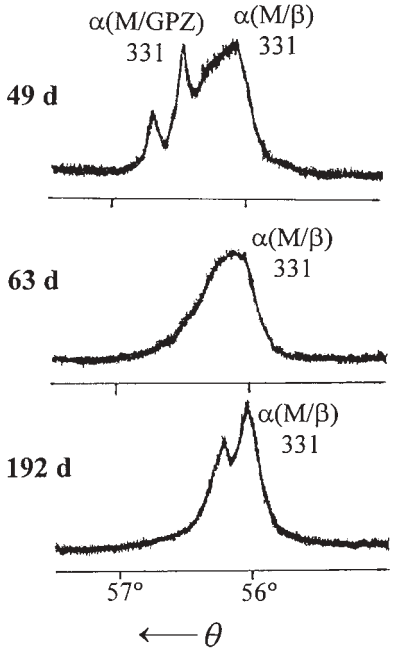

Figure 6. Diffraction lines of the Al-Zn (x_{Zn} = 24%) alloy, quenched from 673 K in water at RT and aged at RT for 49 d, 63 d and 192 d. Samples: fine powder.

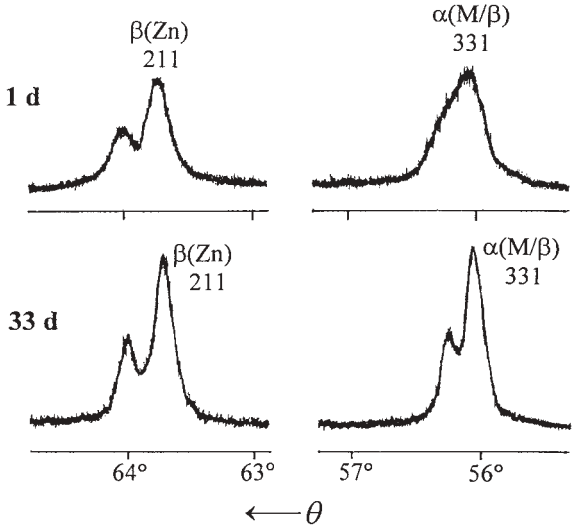

Figure 7. Diffraction lines of the Al-Zn (x_{Zn} = 24%) alloy, quenched from 673 K in water at RT, aged at RT for 1 d and subsequently aged at 333 K for 1 d and 33 d. Samples: fine powder.

fraction line intensities gradually reach the values belonging to the ones of the slowly cooled sample. The initial development of β(Zn), for the same alloy, with the ageing time at RT, is shown in Figure 9 (details of Figure 8 enlarged). The extrapolation of straight parts of the curves to zero intensity gives values of 3 to 4 d in all cases. This is evidence that GP zones, having reached the critical size, are directly transformed to β(Zn) precipitates, thus enhancing the diffraction line intensities of β(Zn).

After prolonged ageing an equilibrium state is reached, in which the phase α(M/β) is in coexistence with phase β(Zn). Phase α(M/β) exhibits rather sharp diffraction lines; this means that most strains around β(Zn) precipitates are annealed. The lattice constant of the α(M/β) phase is independent of the initial alloy composition, amounting to 4.0469(6) Å at RT. The lattice constants of β(Zn) are close to the ones of pure Zn, a = 2.665(2) Å,

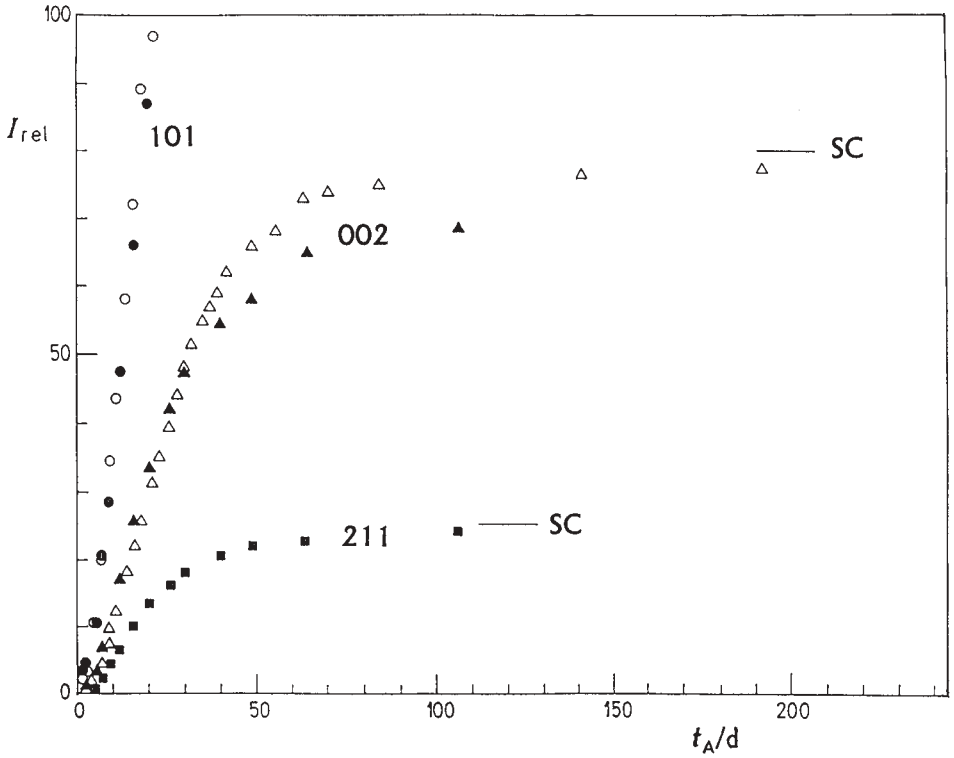

Figure 8. Development of intensities of diffraction lines 101, 002 and 211 of β(Zn) for Al-Zn (x_{Zn} = 24%) alloy, quenched from 623 K (empty marks) and from 653 K (full marks) in water at RT and aged at RT form the time t_A. SC denotes intensities corresponding to the slowly cooled specimens. Samples: fine powder.

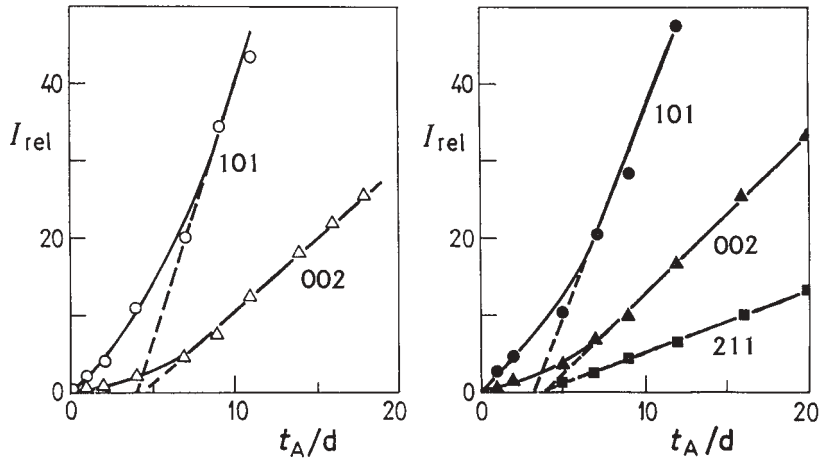

Figure 9. Initial development of intensities of diffraction lines 101, 002 and 211 of β(Zn) for Al-Zn (x_{Zn} = 24%) alloy, quenched from 623 K (the left figure) and from 653 K (the right figure) in water at RT and aged at RT for the time t_A. Samples: fine powder.

c = 4.947(3) Å, c/a = 1.856(3), space group $P6_3/mmc$, at RT. However, for the alloys slowly cooled from the solid-solution temperature to RT, and for the alloys (x_{Zn} = 4.5 and 8%) slowly cooled from 520 K to RT over 15 days, the lattice constant of the α(M/β) phase is 4.0445(10) Å, regardless of the initial alloy composition. The difference between the equilibrium values of the lattice constant of the α(M/β) phase, *i.e.* for the alloys quenched and aged for a prolonged time, and for the slowly cooled alloys, may be explained by different contents of Zn retained in the alloys, as a consequence of different thermal treatments.[4,5]

Thermal Behaviour of the Alloys between RT and T_{ss}

A description follows of dissolution and precipitation phenomena in Al-Zn alloys, having reached the equilibrium state (after quenching and prolonged ageing), exposed to a gradual increase of temperature from RT to the solid solution temperature and then to a gradual decrease of temperature to RT. The alloys having x_{Zn} < 50% and those having x_{Zn} > 50% are described separately.

Alloys with x_{Zn} = 8, 24, 40 and 48%

Prominent diffraction lines at high Bragg angles of Al-Zn (x_{Zn} = 40%) alloy at different temperatures, including both heating and cooling cycles,

are shown in Figure 10. The temperature dependence of the Bragg angle and the relative intensity of diffraction lines at medium Bragg angles of

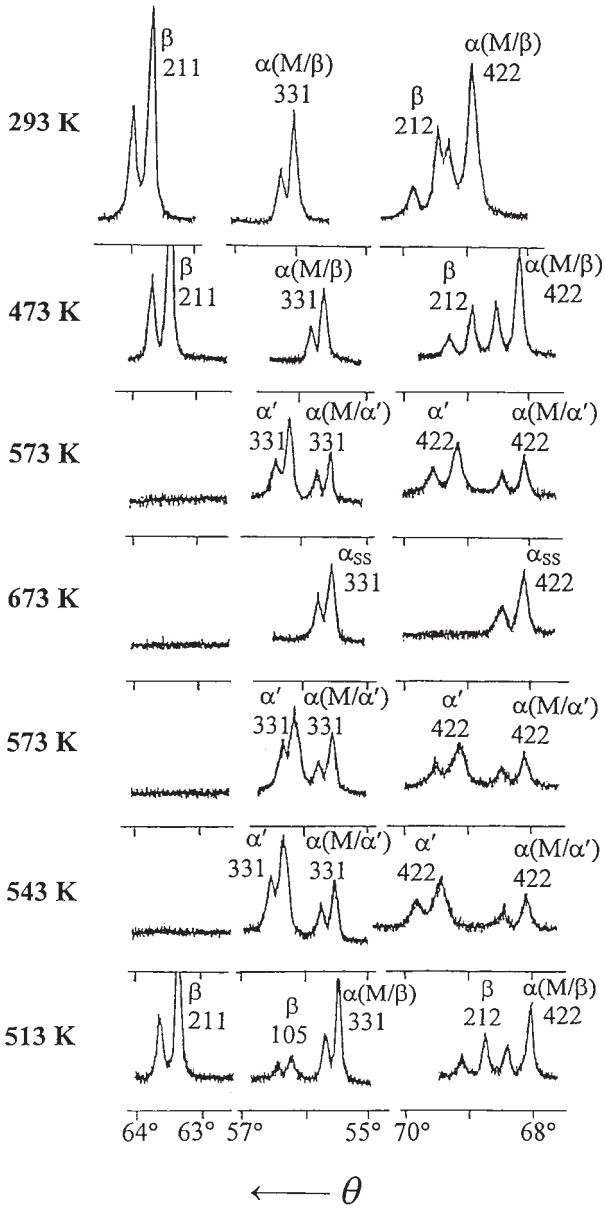

Figure 10. Prominent diffraction lines of Al-Zn (x_{Zn} = 40%) alloy at different temperatures, including both heating and cooling cycles. Samples: fine powder.

Al-Zn (x_{Zn} = 40%) alloy is shown in Figure 11, as well as the angular separation between neighbouring diffraction lines 110 and 103 of β(Zn).

As the temperature of the alloys increases, a decrease of the diffraction line intensities of both α(M/β)- and β(Zn)-phases takes place due to increased thermal vibration amplitudes of the atoms. Also, a gradual shift of diffraction lines toward smaller Bragg angles, caused by thermal expansion, is observed. The Bragg angles of the α(M/β)-phase diffraction lines change linearly up to ≈ 490 K. At higher temperatures, a partial dissolution of β(Zn) in the α(M/β)-phase takes place: this effect compensates or even reverses the shift of the α(M/β)-phase diffraction lines due to thermal expansion. The

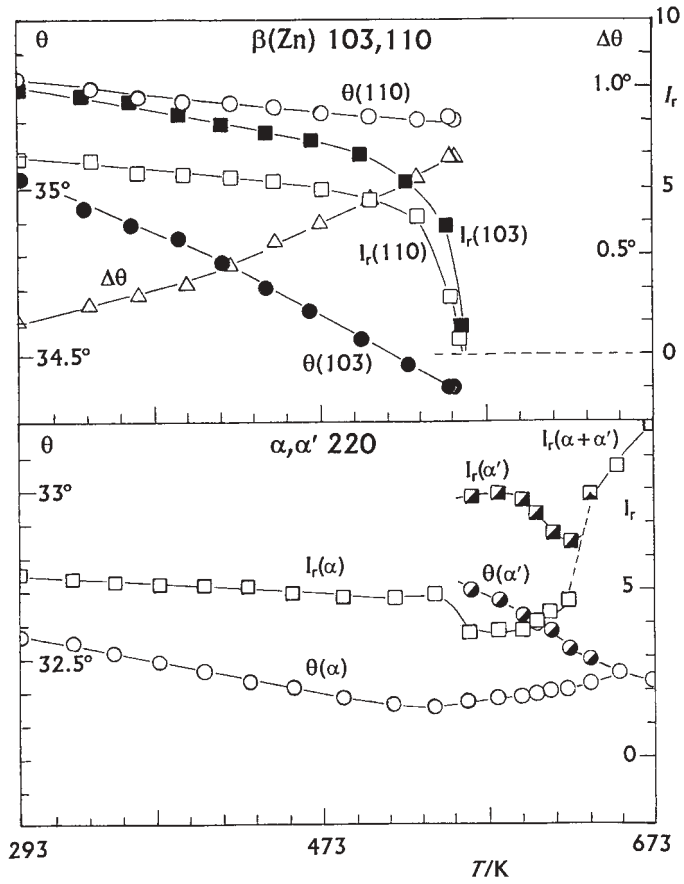

Figure 11. Temperature dependence of the Bragg angle, θ, and the relative intensity, I_r, of prominent diffraction lines for Al-Zn (x_{Zn} = 40%) alloy. The angular separation, $\Delta\theta$, between diffraction lines 110 and 103 of β(Zn) as a function of temperature is also shown.

start of dissolution of β(Zn) is also manifested in an enhanced decrease of its diffraction line intensities (Figures 10, 11).

At about 550 K diffraction lines of β(Zn) abruptly disappear for the alloys with x_{Zn} = 24, 40 and 48%. At the same time, diffraction lines of an *fcc* phase, α′, appear at the high-angle side of all α-phase diffraction lines; the α-phase being now denoted as α(M/α′). The temperature of this phase transition is in agreement with the phase diagram.[1,2] The diffraction line intensities of the α′-phase are bigger the higher is the initial Zn content.

As the temperature further increases, the corresponding diffraction lines of the α′- and α(M/α′)-phases move toward each other, due to a decrease of the zinc content in the α′-phase and an increase of the zinc content in the α(M/α′)-phase. At the same time, the diffraction line intensities of α′-phase decrease. In line with the phase diagram, above ≈ 610 K for the alloy with x_{Zn} of 24%, and above ≈ 650 K for the alloys with x_{Zn} = 40 and 48%, separate diffraction lines of the α′-phase are no longer present. At 673 K, solid solutions of Zn in Al, α_{ss}, for all the studied alloys are detected (Figure 10). The lattice constants of the solid solutions, measured at 673 K, are given in Table II. On cooling, the alloys undergo reversible changes, exhibiting a temperature hysteresis of about 20 K in phase transitions. At a given temperature, the Bragg angles of diffraction lines of the α'- and α(M/α′)-phases are very similar in both the heating and cooling cycles, not depending on the initial Zn content.[6]

Phase β(Zn) exhibits an anisotropy in the thermal expansion (see the temperature dependence of the separation of its diffraction lines 110 and 103 in Figure 11). The following values have been found for the thermal expansion coefficient: α[100] = 1.1(1) × 10^{-5}/K, α[001] = 8.5(9) × 10^{-5}/K. The lattice constants of phase β(Zn) at 548 K (just below the temperature of its transition to α′) are: a = 2.672(3), c = 5.056(6) Å, c/a = 1.89(1).

In line with the phase diagram, the alloy with x_{Zn} = 8% does not exhibit the transition β(Zn) → α′, since for this alloy the region of solid solution is reached at ≈ 490 K. The β(Zn)-phase gradually dissolves in the α(M/β)-phase as the temperature increases, and no traces of its diffraction lines are observed as the temperature reaches the solid-solution region.[6]

Alloys with x_{Zn} = 54 and 62%

Prominent diffraction lines at medium Bragg angles of Al-Zn (x_{Zn} = 54%) alloy at different temperatures, including both heating and cooling cycles, are shown in Figure 12.

Instead of the phase transitions expected according to the phase diagram, namely α(M/β) + β → α′ + α(M/α′) → α_{ss} for Al-Zn (x_{Zn} = 54%) alloy, and α(M/β) + β → α′ + β → α_{ss} for Al-Zn (x_{Zn} = 62%) alloy, the following se-

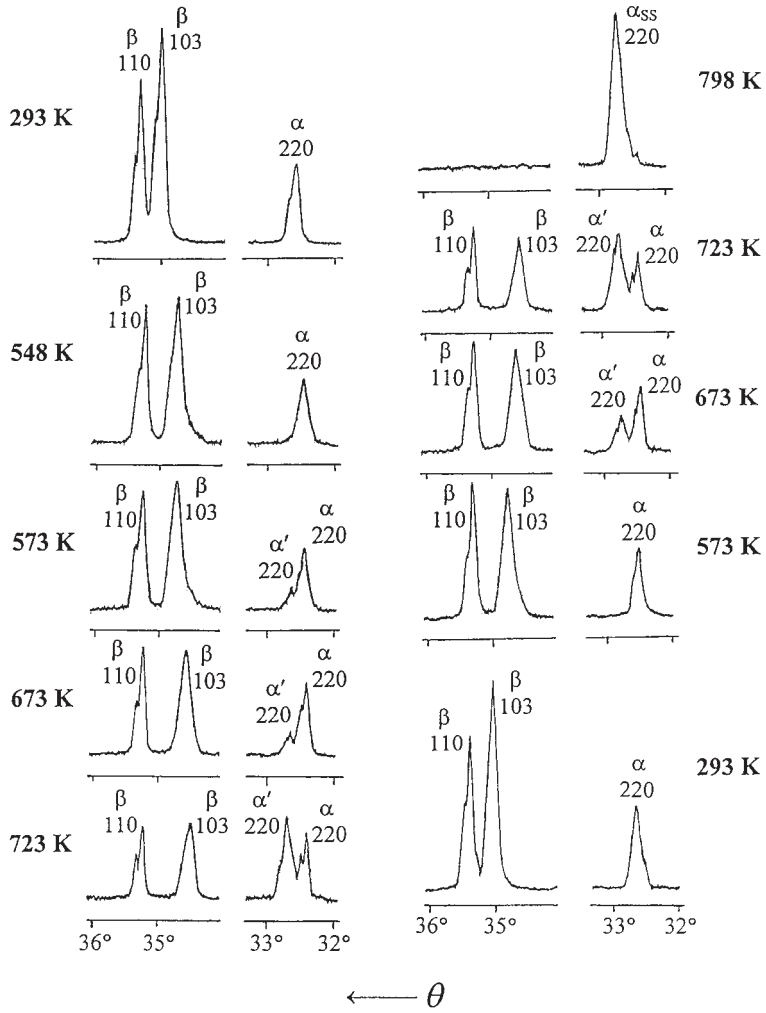

Figure 12. Prominent diffraction lines of Al-Zn (x_{Zn} = 54%) alloy at different temperatures, including both heating and cooling cycles. Samples: fine powder.

quence is observed for both alloys: $\alpha(M/\beta) + \beta \rightarrow \alpha' + \beta + \alpha(M/\alpha',\beta) \rightarrow \alpha' + \beta \rightarrow \alpha_{ss}$ (Figure 12). This indicates that a correction in the phase diagram of the Al-Zn system is necessary.

As the temperature increases, these alloys exhibit similar thermal behaviour as those with lower contents of Zn: thermal expansion of phases $\alpha(M/\beta)$ and $\beta(Zn)$, and anisotropy in thermal expansion of the phase $\beta(Zn)$, and a decrease of diffraction line intensity. Besides, a change of the shape of the $\beta(Zn)$ precipitates on heating is observed, from the broadening of diffrac-

tion lines with $l \neq 0$, *e.g.* 002 and 103, in relation to 100 and 110 (Figure 12). The dimension of the β(Zn) precipitates along the *c* axis decreases as the temperature increases; the Zn atoms, leaving the β(Zn) precipitates, are mainly those which form lattice planes (001).

A pronounced, partial, dissolution of the β(Zn)-phase in the α(M/β)-phase starts at ≈ 490 K. Above ≈ 550 K, a partial transition of the β(Zn)-phase, and probably a partial transition of the α(M/β)-phase, into the fcc α′-phase takes place. The lattice constant of the α′-phase is smaller by ≈ 0.9% than that of the α(M/α′,β)-phase at 560 K, due to different Zn contents in these phases. On further heating, the composition of the phases changes, and the α(M/α′,β)-phase disappears at ≈ 650 K, the α′-phase remaining in coexistence with the β(Zn)-phase. The β(Zn)-phase finally disappears at ≈ 700 K, and the fcc solid solution, α_{ss}, is formed. The lattice constants, $a(\alpha_{ss})$, for the alloys with x_{Zn} of 54 and 62% at 700 K are given in Table II.

TABLE II

$a(\alpha_{ss})$ measured at 673 K or 700 K of the Al-Zn alloys having the initial zinc content x_{Zn}[a]

Temperature/K	x_{Zn} / %	$a(\alpha_{ss})$ / Å
	0 (pure Al)	4.0952(6)
	8	4.0925(8)
673	24	4.0824(7)
	40	4.0692(9)
	48	4.0584(6)
700	54	4.045(1)
	62	4.038(1)

[a] For comparison, the lattice constant of pure Al at 673 K is given.

The same sequence of phase transitions observed in these two alloys indicates that the eutectoid point at ≈ 550 K, shown in the phase diagram at x_{Zn} = 59% for the transition α + β ↔ α′, should be shifted to a point 48% < x_{Zn} < 54%.

In the cooling cycle, a temperature hysteresis in reversal phase transitions is observed. In repeated heating of the same specimen, a temperature delay in phase transitions of several tens K takes place in relation to the first heating. During the second cooling, the microstructural parameters show approximately the same dependence on temperature as during the first cooling and the second heating. This may be explained in terms of the

different microstructure of the sample before the first heating and the second heating. The initial microstructure is formed after rapid quenching of the sample from a temperature above T_{ss} to RT and after a prolonged ageing at RT, resulting in an equilibrium state α(M/β) + β(Zn). One may suppose that precipitates β(Zn) were not uniformly distributed and residual strains in the α(M/β)-phase around the β(Zn) precipitates are present. The first heating of the sample is slow, at a rate of ≈ 2 K/min, and the sample is held for 15 min at a number of temperatures in order to take diffraction patterns. Therefore, one may suppose that the strains are annealed during the first heating. The first cooling is performed in a similar way. This resulted in a microstructure different from the initial microstructure, concerning the size and shape of the β(Zn) precipitates, their distribution in the matrix,

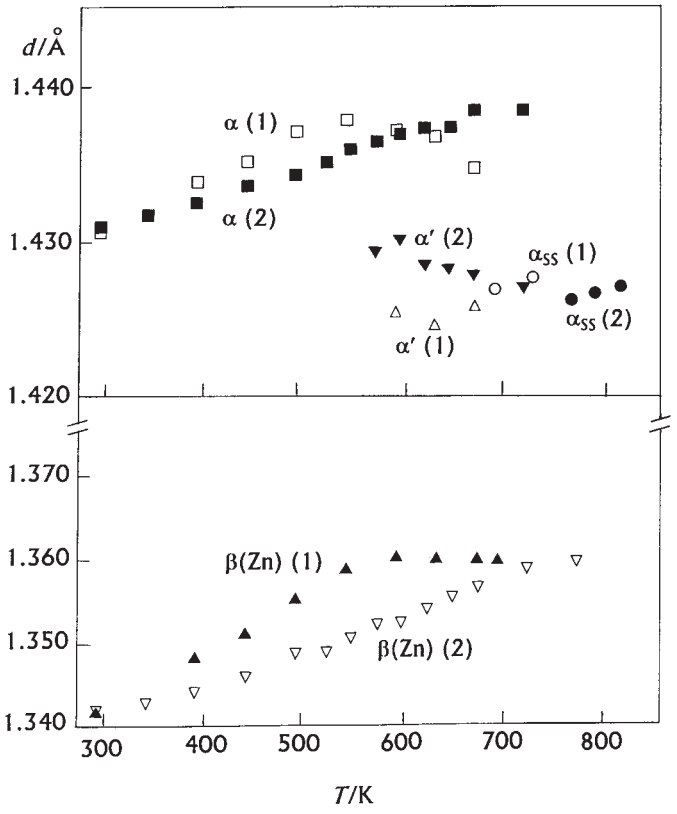

Figure 13. Dependence of spacing $d(220)$ of phases α, α′ and α_{ss} (upper figure), and of spacing $d(103)$ of phase β(Zn) (lower figure), in Al-Zn (x_{Zn} = 54%) alloy, on temperature during the first (1) and second (2) heating of the same specimen (without points corresponding to the cooling cycles).

and strains in the α(M/β)-phase around the β(Zn) precipitates. The strains are mostly annealed during the first slow heating and slow cooling of the sample. A very important fact is that the number of vacancies at RT after the slow heating and cooling cycles may be much smaller than that in the as-quenched sample, which fact has a dominant influence on the diffusion rate of Zn atoms, explaining the delay in phase transitions during the second heating.

As an example, Figure 13 shows the temperature dependence of spacing $d(220)$ of phases α, α′ and α_{ss}, and spacing $d(103)$ of phase β(Zn), in Al-Zn (x_{Zn} = 54%) alloy, during the first and the second heating. One may conclude that the dependence of the microstructural parameters on temperature during the first and the second heating is obviously different.

CONCLUSION

The present paper shows that a detailed and accurate investigation of Al-Zn alloys by means of X-ray powder diffraction has revealed a lot of new information on the microstructure of the alloys, in dependence on the composition, temperature and thermal treatment. The alloys of different composition, quenched rapidly from the solid-solution temperature to RT, have been subjected to ageing, at RT or at elevated temperature, and the precipitation processes, that is, the decomposition of the supersaturated solid solutions, have been studied. Also, the alloys of different composition, having reached the equilibrium state, have been gradually heated from RT to the solid solution temperature and cooled back to RT, and their microstructure has been followed *in situ* by XRD. The present study has proved that accurate measurements of positions and profiles of diffraction lines have been very useful to obtain new information, *e.g.* on the zinc content in the matrix, for different types of precipitates, on the effect of strains occurring at the matrix/precipitate interfaces on the lattice constant of the matrix, on the lattice constants of the intermediate phase α′ and of the solid solution, on the lattice constants of the equilibrium phase β(Zn). It has been shown that previous thermal treatment has a dominant influence on the microstructure of the alloys. Also, the present study has checked the validity of the phase diagram of the Al-Zn system. In order to suggest a definite change in the phase diagram in the region $x_{Zn} > 50\%$, additional studies with different Al-Zn alloys are necessary.

Acknowledgment. – The authors are grateful to Professor Emeritus Hans Löffler for the joint investigation of the Al-Zn alloys and for his long-term interest in this work, as well as to Dr. sc. Gottfried Wendrock, both with the Martin-Luther-Universität, Halle-Wittenberg, Germany (where TEM and SAXS investigations were performed, which confirmed the XRD results obtained in Zagreb; see Refs. 4–7, 9).

Note. – The results described in the present paper were presented in parts at several scientific meetings, the more recent and important ones being the following:
– 14th European Crystallographic Meeting, Enschede 1992 (Book of abstracts, P. Čapkova (Ed.), University of Twente, abstract p. 104);
– 5th Slovenian-Croatian Crystallographic Meeting, Zreče 1996 (Book of abstracts, L. Golič, I. Leban, and A. Golobič (Eds.), University of Ljubljana, abstract p. 50);
– 15th Meeting of Croatian Chemists and Chemical Engineers, Opatija 1997 (Book of abstracts, M. Gojo, N. Trajkov, and S. Smolec (Eds.), Croatian Society of Chemical Engineers, abstract p. A49);
– 6th European Powder Diffraction Conference, Budapest 1998 (Book of abstracts, E. Sváb (Ed.), Technical University of Budapest, abstract p. 95).

REFERENCES

1. H. Löffler (Ed.), *Structure and Structure Development in Al-Zn Alloys*, Akademie Verlag, Berlin, 1995.
2. H. Löffler, G. Wendrock, and O. Simmich, *Phys. Stat. Sol*. (a) **132** (1992) 339–352.
3. S. Popović, *Cryst. Res. Technol*. **20** (1985) 552–555.
4. S. Popović, H. Löffler, B. Gržeta, G. Wendrock, and P. Czurratis, *Phys. Stat. Sol*. (a) **111** (1989) 417–429.
5. S. Popović, B. Gržeta, V. Ilakovac, R. Kroggel, G. Wendrock, and H. Löffler, *Phys. Stat. Sol*. (a) **130** (1992) 273–292.
6. S. Popović, B. Gržeta, H. Löffler, and G. Wendrock, *Phys. Stat. Sol*. (a) **140** (1993) 341–352.
7. S. Popović, B. Gržeta, V. Ilakovac, H. Löffler, and G. Wendrock, *Phys. Stat. Sol*. (a) **141** (1994) 43–52.
8. S. Popović, B. Gržeta, H. Löffler, and G. Wendrock, *Fizika A* **4** (1995) 529–538.
9. S. Popović, B. Gržeta, H. Löffler, and G. Wendrock, *Lattice Constant of the Al-rich fcc α-Phase in Contact with Various Kinds of Precipitates*, in: H. Löffler (Ed.), *Structure and Structure Development in Al-Zn Alloys*, Akademie Verlag, Berlin, 1995, pp. 212–241.
10. S. Popović and B. Gržeta, *Mater. Sci. Forum*, accepted for publication.
11. J. L. Murray, *Bull. Alloy Phase Diagrams* **4** (1983) 55.
12. M. Simerska and V. Syneček, *Acta Crystallogr., Sect. A* **31** (S3) (1983) 185.
13. S. Popović and D. E. Passoja, *J. Appl. Crystallogr.* **4** (1971) 427–434.
14. D. E. Passoya, S. Popović, and P. Barrand, *Met. Trans*. **5** (1974) 715–721.
15. S. Popović, *Cryst. Res. Technol*. **19** (1984) 1351–1358.

SAŽETAK

Pojave precipitacije i otapanja u slitinama Al-Zn

Stanko Popović i Biserka Gržeta

Mikrostruktura slitina Al-Zn, s atomnim udjelom Zn, $x_{Zn} \leq 62\%$, istraživana je s pomoću rentgenske difrakcije u ovisnosti o sastavu, temperaturi i prethodnoj termičkoj obradbi. Pojave precipitacije u slitinama, koje su bile u prezasićenom stanju postignutomu brzim kaljenjem od temperature čvrste otopine (T_{ss}) u vodu sobne temperature, praćene su u ovisnosti o vremenu starenja pri sobnoj ili pri povišenoj temperaturi. Ravnotežno stanje, dosegnuto starenjem, uspoređeno je sa stanjem dobivenim sporim hlađenjem od T_{ss} do sobne temperature. Fazne pretvorbe, pojave otapanja i precipitacije u slitinama, koje su bile u ravnotežnom stanju, proučavane su *in situ* u ovisnosti o temperaturi, od sobne temperature do T_{ss}. Opažena je temperaturna histereza za obratne fazne pretvorbe pri snižavanju temperature od T_{ss} do sobne temperature. Ponovnim grijanjem i hlađenjem utvrđeno je da je mikrostruktura različita u slitinama što su imale različitu termičku obradbu između sobne temperature i T_{ss}. Ukazuje se na nužnost izmjene faznog dijagrama sustava Al-Zn u području $x_{Zn} > 50\%$.